Title

CHARACTERIZATION OF CRYOGENIC Fe-6Ni STEEL FRACTURE MODES: A THREE DIMENSIONAL QUANTITATIVE ANALYSIS

Author

Morris, J.W.

Publication Date

1984-05-01

Lawrence Berkeley Laboratory
UNIVERSITY OF CALIFORNIA

Materials & Molecular Research Division

Submitted to Metallurgical Transactions

CHARACTERIZATION OF CRYOGENIC Fe-6Ni STEEL FRACTURE MODES: A THREE DIMENSIONAL QUANTITATIVE ANALYSIS

G.O. Fior and J.W. Morris, Jr.

May 1984

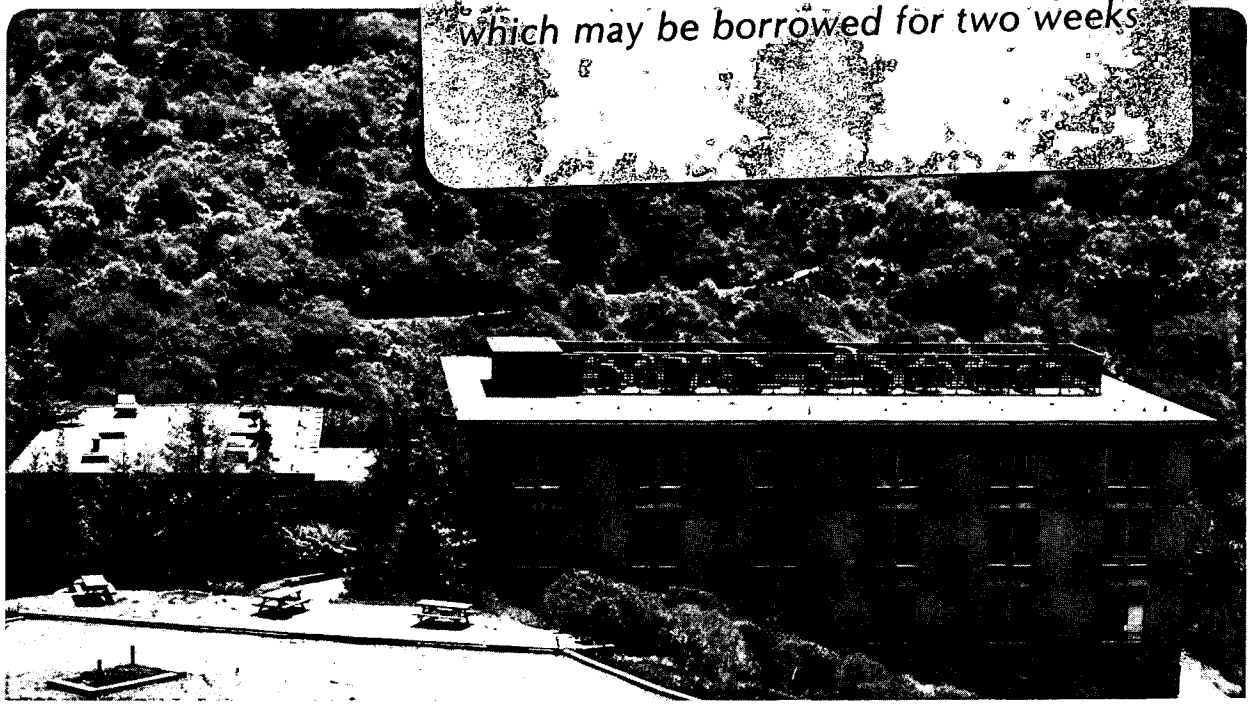

Prepared for the U.S. Department of Energy under Contract DE-AC03-76SF00098

DISCLAIMER

CHARACTERIZATION OF CRYOGENIC Fe-6Ni STEEL FRACTURE MODES: A THREE DIMENSIONAL QUANTITATIVE ANALYSIS*

G. O. Fior and J.W. Morris, Jr.

Materials and Molecular Research Division
Lawrence Berkeley Laboratory
University of California, Berkeley, CA 94720

*This work was supported by the Director, Office of Energy Research, Office of Development and Technology, Magnetic Systems Division of the U.S. Department of Energy under contract number DE-AC03-76SF00098.

CHARACTERIZATION OF CRYOGENIC Fe-6Ni STEEL FRACTURE MODES: A THREE DIMENSIONAL QUANTITATIVE ANALYSIS.

G. O. Fior, J. W. Morris, Jr.

Materials and Molecular Research Division

Lawrence Berkeley Laboratory

University of California, Berkeley, CA 94720

ABSTRACT

Quantitative three dimensional analyses of fracture surfaces on *Fe–6Ni* cryogenic steel were used to study the effect of temperature variations on the geometry of the characteristic features in different fracture modes. Stereo SEM techniques combined with stereo photogrametry provide the tools to perform such analysis on standard Charpy specimens tested with appropriate instrumentation over a 300 degree temperature range. The characteristic features of the ductile fracture mode were found to maintain a constant aspect ratio for these temperatures, while the brittle fracture modes exhibit an aspect ratio that is temperature dependent. This geometrical factor dependence of temperature in

the non ductile case resembles that of the Charpy impact energy for the same temperature range. Based on these findings and on the classical stress-temperature dependence diagram, better known as the *Joffee diagram*, a detailed description of the *ductile-to-brittle* transition is discussed.

May 10, 1984

CHARACTERIZATION OF CRYOGENIC Fe-6Ni STEEL FRACTURE MODES: A THREE DIMENSIONAL QUANTITATIVE ANALYSIS.

G. O. Fior, J. W. Morris, Jr.

Materials and Molecular Research Division

Lawrence Berkeley Laboratory

University of California, Berkeley, CA 94720

I. INTRODUCTION

Today's development of new materials to meet innovative technological applications demands knowledge of the complex processes of fracture that take place under varied testing conditions. This is of particular importance in the development of materials for use at cryogenic temperatures where the *ductile-to-brittle transition* (*DBT*) may occur. Precise understanding of the fracture mechanisms is needed to predict and control the *DBT* for alloy design purposes.

Fracture surfaces represent the final state of a very fast action that occurs in a subject material. The sequence of events during fracture are of an atomic order and are difficult, if not impossible, to observe as they proceed. In studying the mechanism(s) of fracture, we are therefore confined to varying the initial set of conditions, e.g., testing temperature, stress level, loading mode, etc. and observing the end result, i.e., fracture surfaces. Despite this

limited information, past research has provided many interpretations and descriptions of fracture mechanisms. For *DBT* fracture mechanisms in particular, two different models have gained major support:

- One model assumes that there is only one fracture mechanism operating in the transitional stage from ductile to brittle mode. This mechanism result in different fracture appearances at various testing temperatures because of the difference in the amount of plastic deformation that occurs before fracture is completed.

- The other model instead, assumes that there are two different fracture mechanisms, each being fully activated at opposite ends of the temperature scale. This dual mechanism model results in a mixture of two modes of fracture being simultaneously present at intermediate temperatures when each mechanism is only partially activated.

Therefore, an investigation of the fracture mechanism(s) that operate within the *DBT* regime shall be performed through a more complete analysis of resulting fracture surfaces. Such analysis should derive from accurate surface measurements in order to characterize the geometry of the features present. Conventional ($2D$) scanning electron microscope (*SEM*) observations of the fracture surface can qualitatively distinguish the characteristic geometry of different features. The use of stereo imaging techniques to obtain three dimensional ($3D$) qualitative and quantitative information on fracture surface, however, can effectively extend the perception of the real fracture appearance by revealing additional information about depth, roughness, curvature, etc., that conventional $2D$ images cannot provide. In this work, a quantitative $3D$ fractographic analysis of cryogenic steel is used to characterize the fracture modes of an $Fe-6Ni$ alloy over the range of temperature where its *DBT* occurs.

II. EXPERIMENTAL PROCEDURE

A. *Material and Heat Treatment*

The material used for this study was a commercial steel obtained from the *Nippon Steel Corporation* in the form of a one-inch thick plate. The chemical composition (in weight%) of this alloy was as follows: C=.063; Mn=1.21; Si=0.029; P=0.008; S=0.01; Ni=5.86; Cr=0.69; Mo=0.20 Fe=balance. This alloy is designed for cryogenic applications since it maintains its high strength and high toughness at low temperatures. Normally this alloy is given the conventional quenching and L-tempering (*QLT*) heat treatment[1] or the two B-tempering (*2BT*) treatment[2-4] in order to depress the ductile to brittle transition temperature (*DBTT*) to even lower temperatures. For this work, however, easy access to testing temperatures below and above the *DBTT* was desired. Therefore, the material was annealed at 1000°C for two hours to remove any previous thermomechanical treatment and then water quenched (*WQ*) to raise the *DBTT* above liquid nitrogen temperature.

B. *Mechanical Test*

Standard V-notch Charpy specimens were cut from the *WQ* plate with the longitudinal axis parallel to the rolling direction and the loading direction perpendicular to it. Three or more specimens were tested at each temperature, varying from 77 K to 373 K. Subzero temperatures were obtained using different proportions of liquid nitrogen, isopentane (2-methyl butane) and methyl alcohol. Charpy impact tests at subzero temperatures were performed following standard procedures of *ASTM* #23-72. The tests were conducted in a *Tinius Olsen M*64 Charpy machine, instrumented with a *DYNATUP* 500 system to monitor the dynamic behavior and record both load and absorbed energy at any time during the test. The hammer striking velocity was $512 cms^{-1}$ for all

tests, and the procedure used for the instrumented Charpy tests followed the recently proposed standard method.[5] Upon calibration of the instrumentation, a very good agreement was always obtained between the absorbed energy measured from the dial and from the oscilloscope display.

C. *Stereo Scanning Electron Microscopy*

The specimens fracture surfaces were directly observed in the *SEM*. A special design and custom built sample holder was used to position the full size specimens always with their fracture surface normal to the incident electron beam. Magnification was calibrated for X and Y axes and was checked before each session with a standard calibration grid. The *SEM* used had an eucentric* specimen tilt stage with ±.5 degree accuracy. Stereo pairs of fractographs were taken using the specimen tilting method.[6] The specimen was tilted symmetrically across the flat surface to minimize distortion of the images and to simplify $3D$ equations by using the central plane image equal to zero tilt.[7,8] The optimum total tilt angle was experimentally determined to be 10 degrees for the given characteristics of the stereoscope focal length, material topographic configuration and operator interpupillary distance.[9] Magnification was held constant at $2000X$, which allowed for enough resolution of all present features and permitted the use of the parallel projection approximation for the extraction of $3D$ information.[10,11]

D. *Stereo Measurements*

Stereo pairs of *SEM* fractographs were observed under a *WILD ST4* mirror stereoscope. In this work a 1224 *Numonics* digitizer was used to obtain all parallaxes (difference in length between two points as they are recorded in

* Eucentric is the generally accepted term used to describe a specimen stage in which the tilt axis, rotation axis and optical axis intersect each other in one point, allowing for specimen tilt and rotation without the need for readjusting either the specimen position or the focus.

different tilted photographs) and other measurements from the fractographs. Digital display and printed record of the measurements were automatically produced at the same time the data was stored in a terminal bubble memory through a digitizer-terminal interface. Later, data groups were sent via telephone line to the central computer facility where a program in *BASIC* written by the authors processed the information to generate all 3*D* parameters, statistical analyses and graphics.[12] Figure 1 shows a flow chart of this measuring process.

E. *Sampling*

The fracture surface appearance of Charpy impact specimens at four different testing temperatures as seen in the *SEM* are shown in Figure 2. From these 2*D* fractographs, two results are noteworthy. First there is a definite change of predominant fracture mode, and second, there is an infinite number of different shapes of features present within each fracture mode. In order to classify these features, a very restricted definition was chosen so that no subjective judgement was required from the operator. The definition specified in this work divides the features in two categories:

Ductile Dimples (*DD*): a void of concave shape with a protuberant edge or border ridge such that if starting from an initial point P one may follow it in any direction and return back to the same point P, circumscribing the void completely and without interruptions. Such edges are clearly observable in *SEM* fractographs given the higher contrast produced by the pronounced height also known as the ***edge effect***.[13]

remaining Features (*RF*): features that fail to be classified as *DD* will be considered *RF* for the purpose of this work.

Figure 3 illustrates some examples of *DD* and *RF* according with the definition

given above. For each sampled feature a total of four data numbers were obtained:

i) Class *DD* or *RF* (dummy variable): this data was obtained through the stereoscope by the operator using the adopted convention and recorded via the keyboard into the terminal's bubble memory.

ii) Projected Area *A*: defined as the area circumscribed by the edge or ridge of the feature. It was directly measured with the digitizer using the stereoscope and corrected later by the topographic curvature angle.

iii) Maximum Depth *Z*: defined as the difference in height between the top and the bottom of the center of the feature. This parameter was calculated from the measurement of the parallaxes taken with the digitizer and stereoscope.

iv) Topographic Curvature: defined as the angle of inclination of the feature with respect to the normal to the fracture surface (also referred to as the central plane). This parameter is also calculated from parallaxes measured with the digitizer and stereoscope.

Figure 4 shows an idealized fracture profile with the 3*D* parameters as measured in this work. The relation between the difference in height or elevation and the parallax measurements taken with the digitizer are given by the following equation:

$$Z_c = \frac{P}{2 \times \sin \alpha} \qquad (1)$$

where:

Z_c = difference in height referred to the central plane

P = parallax value

α = half of the total tilt angle between left and right fractographs

Introducing the magnification M of the fractographs (1) becomes:

$$Z_c = \frac{P}{2 \times M \times \sin \alpha} = \frac{P}{k} \qquad (2)$$

where:

$k = 2 \times M \times \sin \alpha =$ constant throughout this work

The above equations are derived assuming parallel projection (M>500) [6-9,11,14]

Even with the automation implemented for the measuring process, the number of features makes it virtually impossible to sample the whole fracture surface of the specimens at the magnification selected (2000X). Instead, a random sampling technique was used, in which both the stereo fractographs and the features measured were selected after computer generated random coordinates were obtained for each specimen. Twelve random features were measured for each of six different stereo pairs of fractographs randomly taken within the central area of each specimen at six different testing temperatures.

IV. RESULTS

A. *Mechanical Properties*

As desired and expected from the material heat treatment combination, the Charpy impact tests showed a gradual ductile to brittle transition of the total absorbed energy measured with the instrumented tup. The load-time history of these tests can also provide a good estimate of crack nucleation and propagation energies.[15,16] Figure 5 summarizes the information obtained from the instrumented Charpy tests over a 300 degrees temperature range. Defining the *DBTT* as the temperature corresponding to the midpoint between the upper and lower shelves, it is found that for both total absorbed energy E_a and estimated crack propagation energy E_p the *DBTT* was approximately 150 K. The parameters E_a and E_p also show a wide transition region. The estimated crack nucleation energy E_n instead has a narrower transition region with a very well

defined upper shelf that drops at about 175 K to give a *DBTT* of 125 K. In the brittle region it was observed that E_n accounts for more than 90% of the total energy absorbed by the specimens. The plot of E_n *vs.* T in Figure 5, suggests that the fracture nucleation mechanism is virtually the same down to 170 K. This result of the mechanical behavior, if correct, should also be found in the proposed fracture analysis.

B. *Fracture Surface Analysis*

1. *Projected Area* **A**:

The average projected area A of the features sampled in the fracture surface was found to decrease with increasing testing temperatures (Figure 6). The plot $\frac{1}{A}$ *vs.* T shows a *DBT* shape with a transition temperature of 170 K.

2. *Maximum Depth* **Z**:

The average maximum depth Z for all the features was found to increase with increasing testing temperature. The plot of Z *vs.* T also follows a *DBT* shape with a transition temperature of 170 K (see Figure 7).

3. *Aspect Ratio* **V**:

Given the characteristics of projected area A and maximum depth Z found in this work, it seems appropriate to define an aspect ratio V that incorporates both geometrical parameters A and Z. V was defined as the ratio of Z and the square root of A

$$V = \frac{Z}{\sqrt{A}} \tag{3}$$

The plot of the calculated V *vs.* T is given in Figure 8. Its *DBT* shape can be verified using the histogram shown in Figure 9. Separate curves of V for *DD* and *RF* are plotted in Figure 10 and their histograms are presented in Figures

11 and 12. The plot of V_{DD} does not show any dependence on temperature, while for V_{RF} there is a very smooth *DBT* region with a *DBTT* at about 175*K*.

4. *Density of Ductile Dimples* ρ:

This variable, defined as the number of ductile dimples per unit of sampled area, shows a very drastic and narrow *DBT* with a transition temperature around 175 K (Figure 13). The combination of this result with the constant geometrical V_{DD} ratio indicates that the effect of low temperature is to inhibit the nucleation of *DD* rather than changing their shape.

5. *Roughness Factor* **F**:

The creation of two new surfaces is inherent to the process of fracture. A portion of the total absorbed energy is consumed by the generation of these free surfaces and therefore some relationship between the energy absorbed and the total surface area must exist. One way of studying this relationship is by introducing a roughness factor F defined as the ratio of the real total area of topographic fracture and its corresponding specimen cross sectional area. The real total area of topographic fracture is estimated as the sum of the measured projected area A plus the area of the feature *wall* defined as the maximum depth Z times the perimeter of the feature which for this purpose is assumed of circular shape:

$$F = \frac{\sum_{i=1}^{n} (A_i + (Z_i \times B_i))}{S} \qquad (4)$$

where:

F = roughness factor (dimensionless)

A_i = projected area of the ith feature (μm^2)

Z_i = maximum depth of the ith feature (μm)

B_i = perimeter of the ith feature (μm)

S = specimen's sampled cross section (μm^2)

Figure 16 shows the graph of F *vs.* T. Here there is a *DBT* with similar characteristics to those obtained from other $3D$ parameters. However, the physical interpretation of F is of greater significance since it contains, by definition, all previously discussed $3D$ parameters and it is directly related to the energy required for fracture to occur.

G. *Statistical Analysis*

The results obtained from the $3D$ quantitative fracture analysis (A,Z,V, *etc.*) , are only statistical estimates of the *true* unknown values. In this work, a parametric statistical method was used to find the level of confidence at which the results were obtained.[17]

Three levels of confidence corresponding to three different interval sizes were found for the projected area A, maximum depth Z and aspect ratio V at each of the six sampled temperatures. For each interval size, the average of the confidence levels over all the different temperatures is shown in Figure 15. From these graphs two general results can be observed. First, the confidence level for V is always greater than for A or Z alone, which implies that their combination into a single parameter strengthens the confidence level. Second, as expected from the definition of *DD* used here, the confidence level is for *DD* > *ALL FEATURES* > *RF*.

A confidence level was also found for the regression line of V_{DD}, which in Figure 10 is shown to be a constant independent of T. The confidence level is 97% for the intercept ±10% interval size and 99.6% for ±20% interval size.

A. *Ductile to Brittle Transition*

A qualitative description of the *DBT* and of the different fracture mechan-

isms involved, with special emphasis on the least understood *quasi-cleavage mode* (*QCM*) can be discussed based on the stress-temperature dependence originally reported by Joffe[18]. A schematic illustration of this dependence adapted to the findings of this work is given in Figure 16. Here the critical cleavage stress σ_c is defined as the stress on the cleavage plane of the most favorably oriented grain.[19]

When testing at high temperatures (*CVN* upper shelf), the stress in the material will first reach the yield level and plastic deformation will begin to occur. Microvoids will nucleate and grow on favorable sites with further deformation. The stress will continue to raise until microcracks form by void coalescence and propagate to complete fracture. This is a purely strain-induced *ductile fracture mode* (Figure 16, $T>T_D$). On the other side of the diagram, at very low temperatures (*CVN* lower shelf), the yield stress is strongly dependent on temperature and much higher than σ_c. In this condition the material will never reach the yield level and therefore no plastic deformation can occur. Microcracks will nucleate first on favorably oriented grains when the stress reaches the critical cleavage level σ_c. As the stress continues to increase, microcracks propagate to other grains to produce a clean undeformed fracture surface. This is a purely stress-induced *cleavage fracture mode* (Figure 16, $T<T_C$).

For intermediate temperatures ($T_C<T<T_D$), if the material reaches first the yield stress level ($T_T<T<T_D$), microvoids will be nucleated on the most favorable sites. As the stress continues to increase, the material strain hardens and some planes of the most favorably oriented grains, which are already deformed to some extent, will reach the critical cleavage stress level and nucleate microcleavage cracks. These cracks will eventually produce general fracture by plastic coalescence with existing microvoids. The resulting fracture surface will

show a predominance of ductile dimples with a few strain-induced cleavage* facets among them. This mode is defined as *quasi-cleavage fracture mode type I* (QC_I). On the other hand, for the lower region of the intermediate temperatures ($T_C<T<T_T$), the critical cleavage stress is reached before yielding and therefore the most favorably oriented grains nucleate microcleavage cracks on preferred planes. These microcracks extend to the boundaries with the less favorably oriented grains where they can not propagate because the stress is not high enough. As the stress increases and passes the yield level, those less favorably oriented grains that remained uncracked will nucleate microvoids by deformation and coalesce with the cleaved planes to produce general fracture. In this case, the fracture surface will be primarily stress-induced cleavage facets with few ductile dimples clustered in small areas among them. This mode is defined as *quasi-cleavage fracture mode type II* (QC_{II}).

Both types of quasi-cleavage fracture consist of a mixture of dimples and cleavage facets, however the amount of each one present is a function of temperature as seen in Figure 13. It is also important to remember that while dimples of both quasi-cleavage types have the same origin (i.e., strain-induced microvoid nucleation, growth and coalescence), the cleavage facets instead are strain-induced for *type I* and stress-induced for *type II*. This different nature of the cleavage in the quasi-cleavage mode is suspected to be responsible for the change of the V_{RF} with temperature shown in Figure 10. By similar argument then, the temperature independence of V_{DD} can be explained.

B. 3D *Characterization of Fracture*

---

* Strain-induced cleavage is a term that describes cleavage produced by a local stress-enhancement that results from strain hardening.

1. *Geometry:*

The aspect ratio, a combined $3D$ parameter, gives expected but nonetheless important information about the characteristics of ductile dimple fracture. As seen in Figure 10, V_{DD} is independent of temperature. This result indicates that the configuration of *DD* must only be a function of the shape and distribution of their nuclei. It is also important to note, however, that temperature, as seen in Figure 13, has a very strong influence on the number of *DD* that are nucleated during the process of fracture.

On the other hand, V_{RF} shows a smooth *DBT* curve (Figure 10) with upper and lower shelves just below V_{DD} and above zero respectively. These two limiting values of V_{RF} are significant in fracture characterization since they separately provide information about the fracture mechanism correlation and about the material microstructure. With the upper limit almost tangent to the constant value of V_{DD}, it is reconfirmed that at high temperature, both *DD* and *RF* are strain-induced fracture modes with the same origins.[19-21] The lower limit instead has a value of approximately .08 for this material and set of initial thermomechanical conditions. This limit value must be a function of the effective grain size and the preferred cleavage plane orientation. There could be, however, more than one equally preferred cleavage plane, or different planes could be preferred at different temperatures which in addition to changing the lower V_{RF} limit may also be an important factor in determining the width and shape of the temperature transition region. Further research combining $3D$ fractographic analysis with metallography is suggested to investigate this topic.

The roughness factor F compiles all the $3D$ quantitative information measured from the specimen. As seen in Figure 16, F follows closely the *DBT* exhibited by the material which is a consequence of its relationship to the total sur-

face area created during the fracture process. The use of this factor F could then be extended as a method to estimate the energy required for fracture, becoming of great usefulness in failure analysis. More expeditious measurements of F could perhaps be attempted using a continuous-flow krypton adsorption method for ultra low surface area measurements.[22,23] Preliminary experiments with this technique show that fracture surface area measurements on Charpy specimens require the maximum sensitivity of the instrumentation. Interpretation of these results still to be determined.

VI. CONCLUSIONS

In a polycrystalline BCC material like the $Fe-6Ni$ steel investigated here, with a relatively homogeneous distribution of nucleation sites for microvoids, the fracture surface appearance would be fully ductile if the testing temperature is high enough to nucleate all the voids. Lower temperatures allow other non-ductile mechanisms to intrude and change the fracture appearance proportionally.

The *ductile dimples* aspect ratio remains constant with temperature, indicating that it may only be a function of the shape and distribution of the *DD* nuclei. The aspect ratio for the *remaining features* instead, exhibit a temperature dependence that follows closely the *DBT* curve of the Charpy impact energy.

The roughness factor F is an indicator of the total fracture surface area that can be used as a $3D$ estimator of the energy required to fracture.

REFERENCES

1. S. Yano, H. Sakurai, H. Mimura, et al.: *Trans. Iron Inst. Japan*, 1973, vol. 13, p. 133.
2. S. Jin, J.W. Morris, Jr. and V.F. Zackay: *Metall. Trans.*, 1975, vol. 6A, p. 141. *(ibid.)*, p.1569.
4. S. Jin, K. Hwang and J.W. Morris, Jr.: *(ibid.)*, p. 1721.
5. R. Ireland: "*Specialist Meeting on Instrumented Precracked Charpy Testing*", EPRI NP-2102-LD, Project 1757-1, CSNI #67, 1981, pp. 1-25.
6. A. Boyde and P.G.T. Howell: *Scanning Electron Microsc.*, 1977, vol. 1, p. 571.
7. B. Hudson: *J. Microsc.*, 1973, vol. 98, p. 396.
8. F.J. Minter and R.C. Piller: *J. Microsc.*, 1979, vol. 117, p. 305.
9. M. Martin, D.A. Ryder and T.J. Davies: *Metallography, 1976, vol. 9, p. 157.*
10. P.G.T. Howell: *Scanning Electron Microsc.*, 1975, vol. 1, p. 697.
11. J.E. Hilliard: *J. Microsc.*, 1972, vol. 95, p. 45.
12. G.O. Fior: *Acta Cient. Venez., Supl. 1981, vol. 1, p. 234.*
13. O.C. Wells: "*Scanning Electron Microscopy*", McGraw-Hill, New York, 1974, p. 113.
14 J.B.F. Cripps and H. Sang: *Rev. Sci. Instrum.*, 1970, vol. 41, p. 1825.
15. T.J. Koppenaal: "*Instrumented Impact Testing*", ASTM, STP #567, 1974, p. 92.
16. H. Kotilainen and E. Sirkkola: Citation #5, 4-3.
17. D.L. Davies and P.L. Goldsmith: "*Statistical Methods in Research and Production*", 4th edition, Oliver & Boyd, Edinburgh, 1972, p. 58.

18. A.F. Joffe: "*The Physics of Crystals*", 1st edition, McGraw-Hill, New York, 1928, p. 58.

19. L. Cienchu, S. Fuyu and L. Fenland: *Acta Metall. Sinica*, 1979, vol. 15, p. 260.

20. AMERICAN SOCIETY FOR METALS: "*Metals Handbook*", 8th edition, 1974, vol. 9, p. 65.

21. C.D. Beachem, B.F. Brown and A.J. Edwards: *US Nav. Res. Lab., Rep. DDC #AD-416457*, **AD- 416457**, 1963.

22. S. Lowell and S. Karp: *Anal. Chem.*, 1972, vol. 44, p. 1706.

23. S. Lowell: *Anal. Chem.*, 1973, vol. 45, p. 1576.

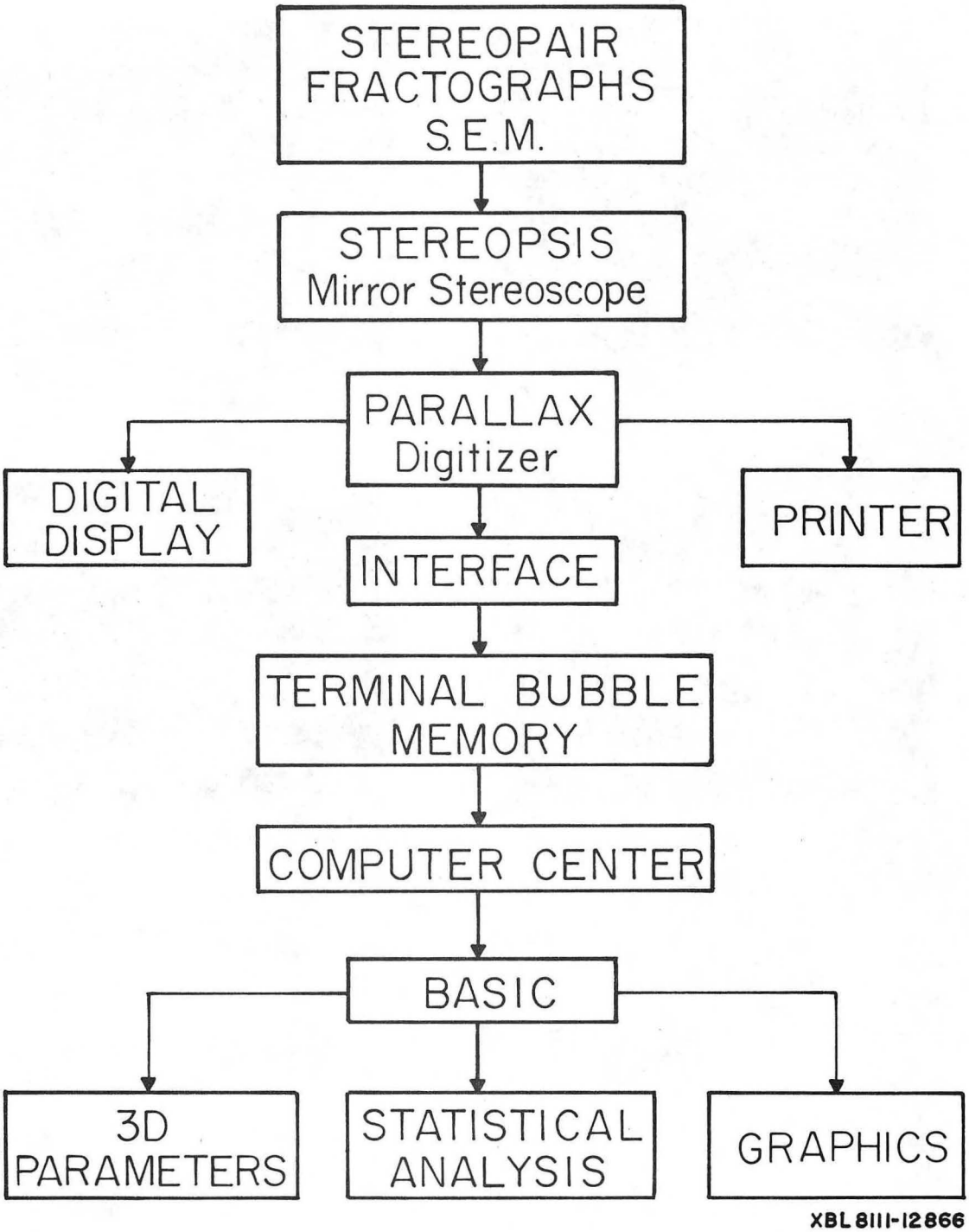

Fig. 1.

Stereoscopic measuring process (flow chart).

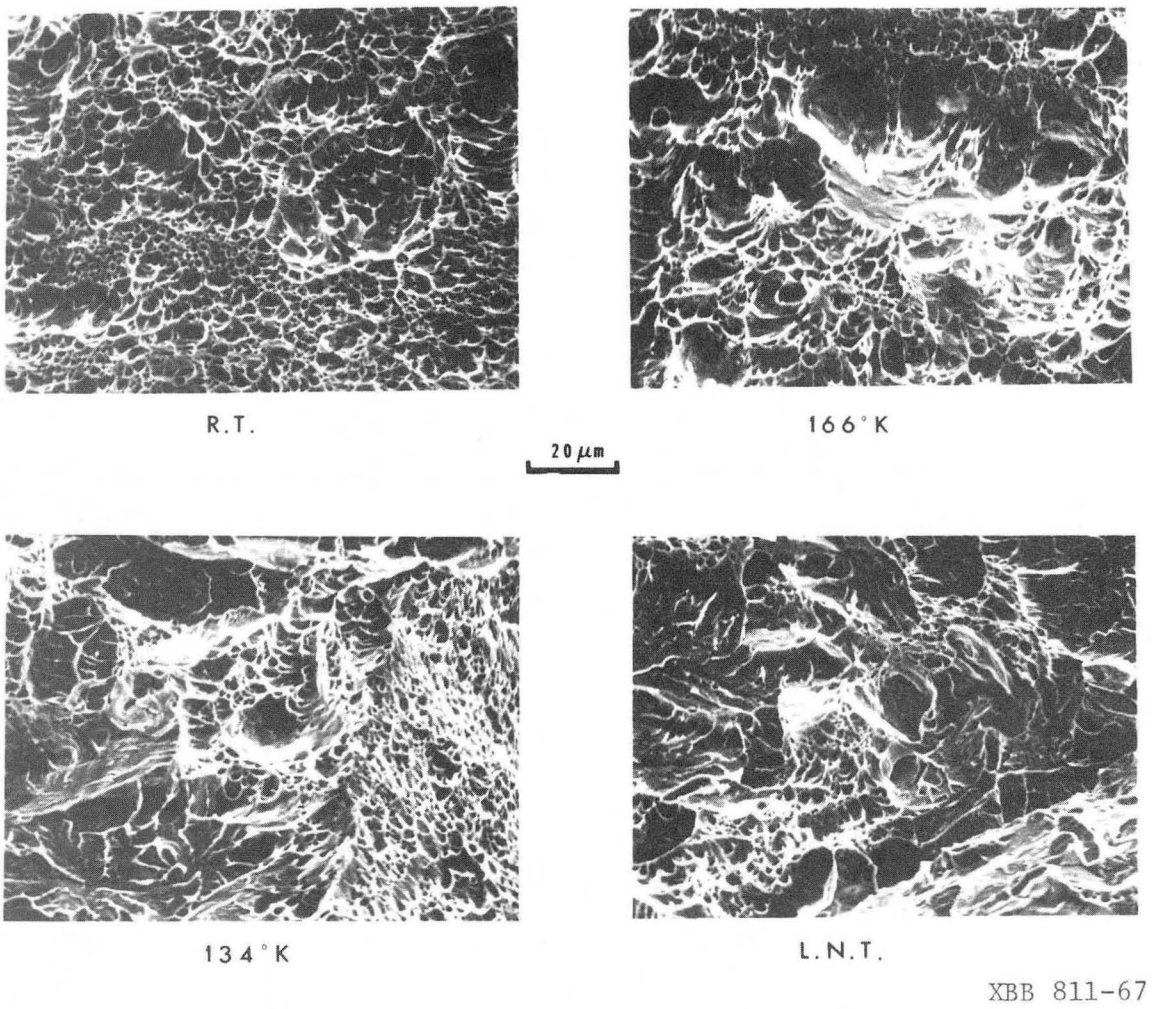

Fig. 2.

SEM fractographs of Charpy specimens.

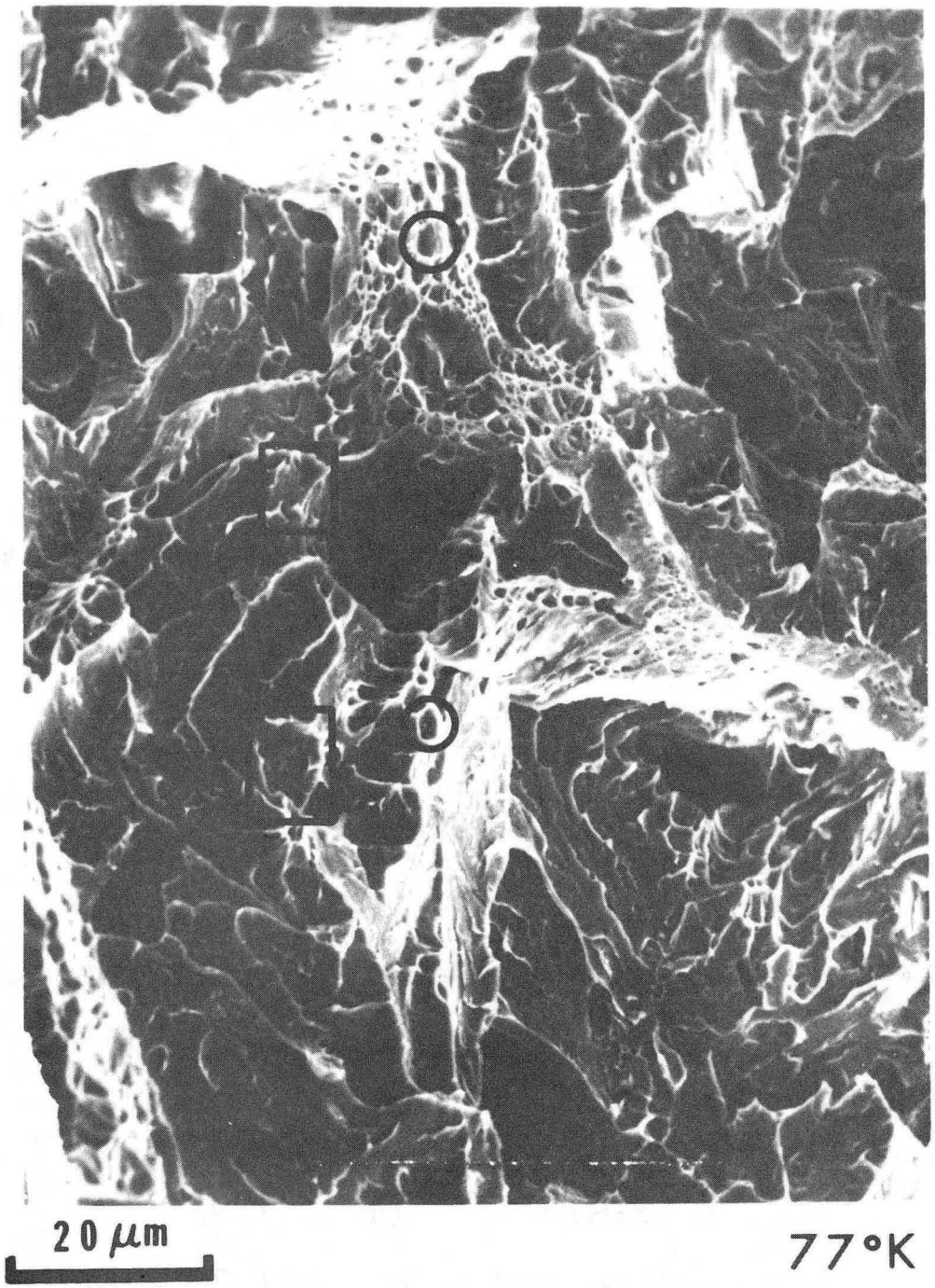

Fig. 3.

SEM fractograph showing *DD* and *RF* according with given definition.

FRACTURE SURFACE PROFILE

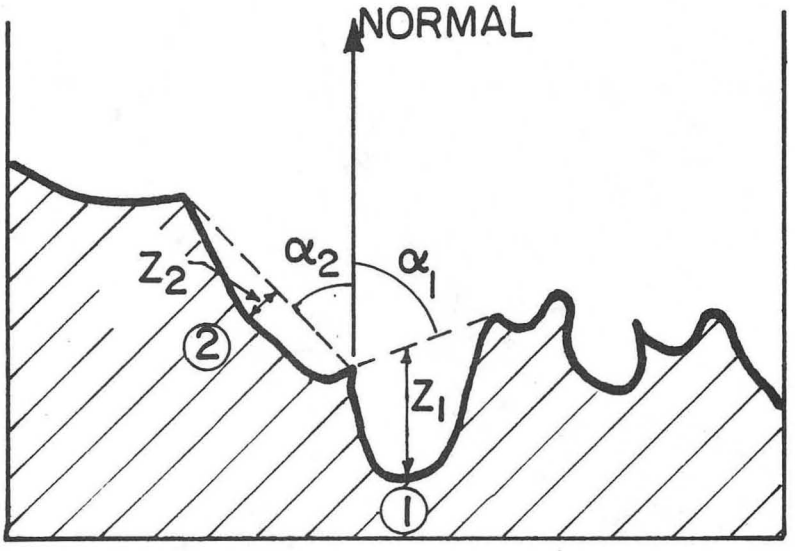

① DUCTILE DIMPLE (DD) PROFILE

② REMAINING FEATURES (RF) PROFILE

3D MEASUREMENTS:

α = ANGLE OF INCLINATION or
TOPOGRAPHIC CURVATURE

Z = DEPTH (DD) or HEIGHT OF RIDGES (RF)

PROJECTED AREA "A" NOT SHOWN

XBL 8111-6943A

Fig. 4.

Schematic fracture profile with 3*D* parameters as measured for *DD* and *RF*.

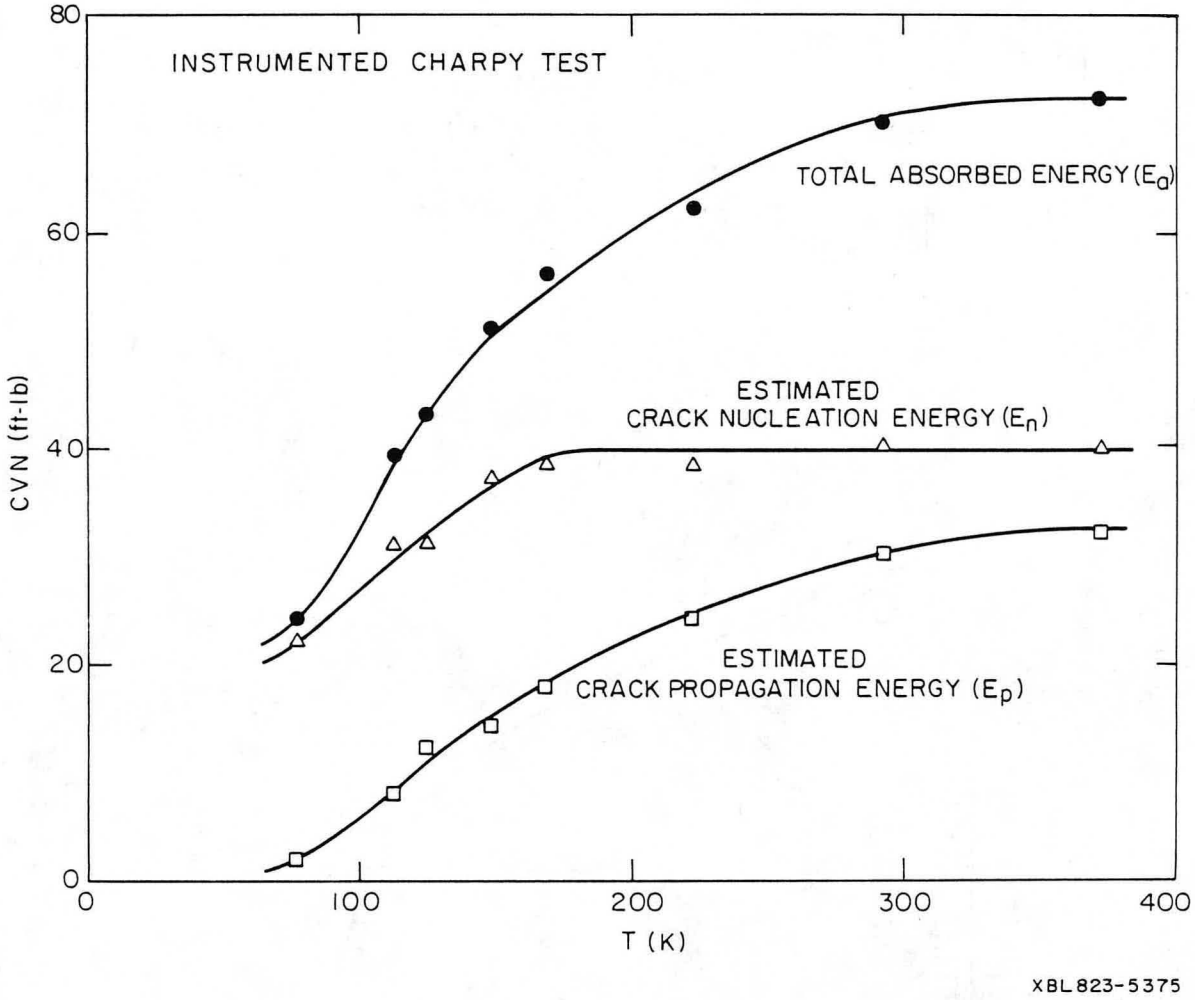

Fig. 5

Charpy impact energy *CVN vs.* temperature.

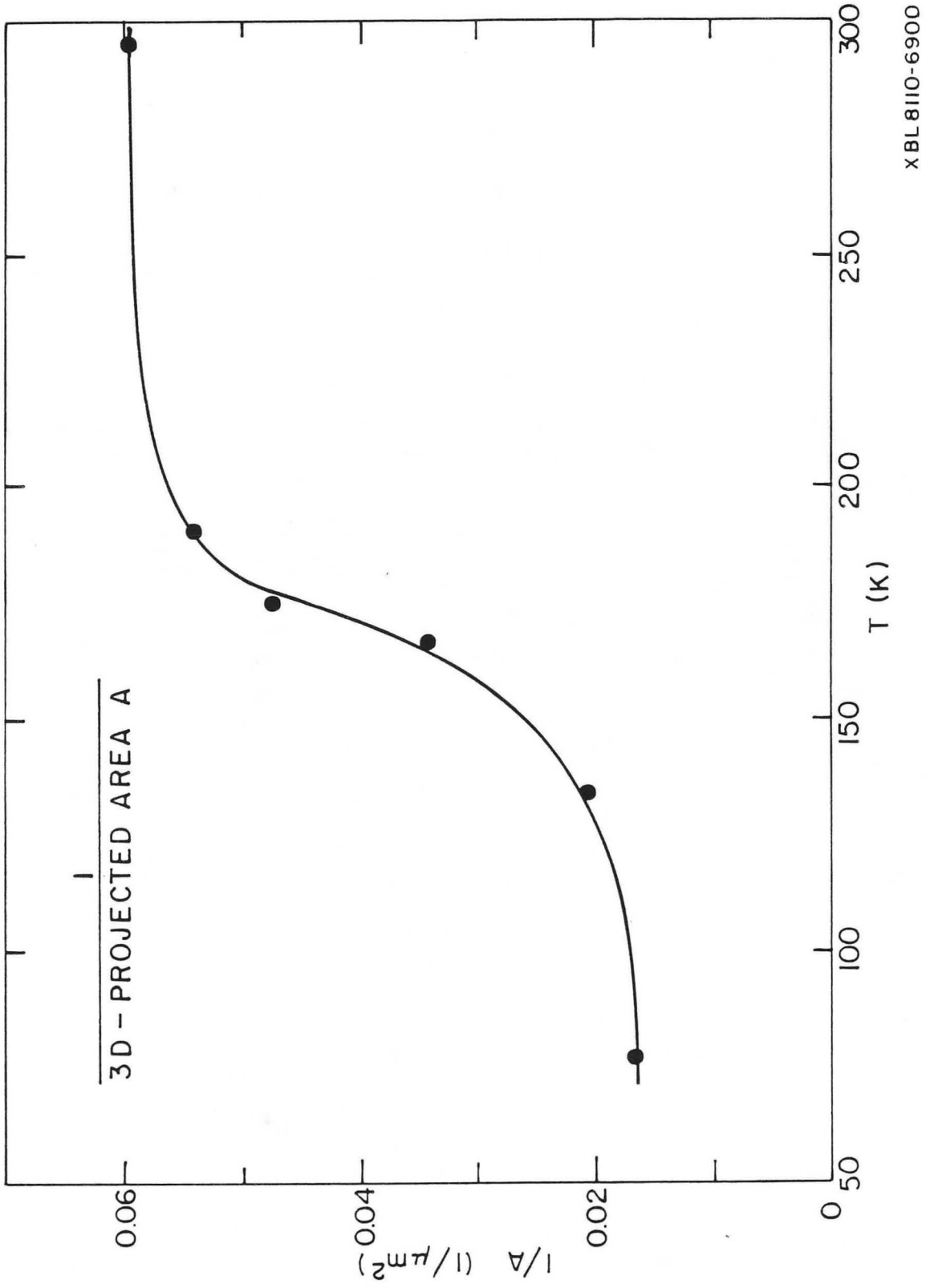

Fig. 6.

Average of $\frac{1}{A}$ *vs.* temperature.

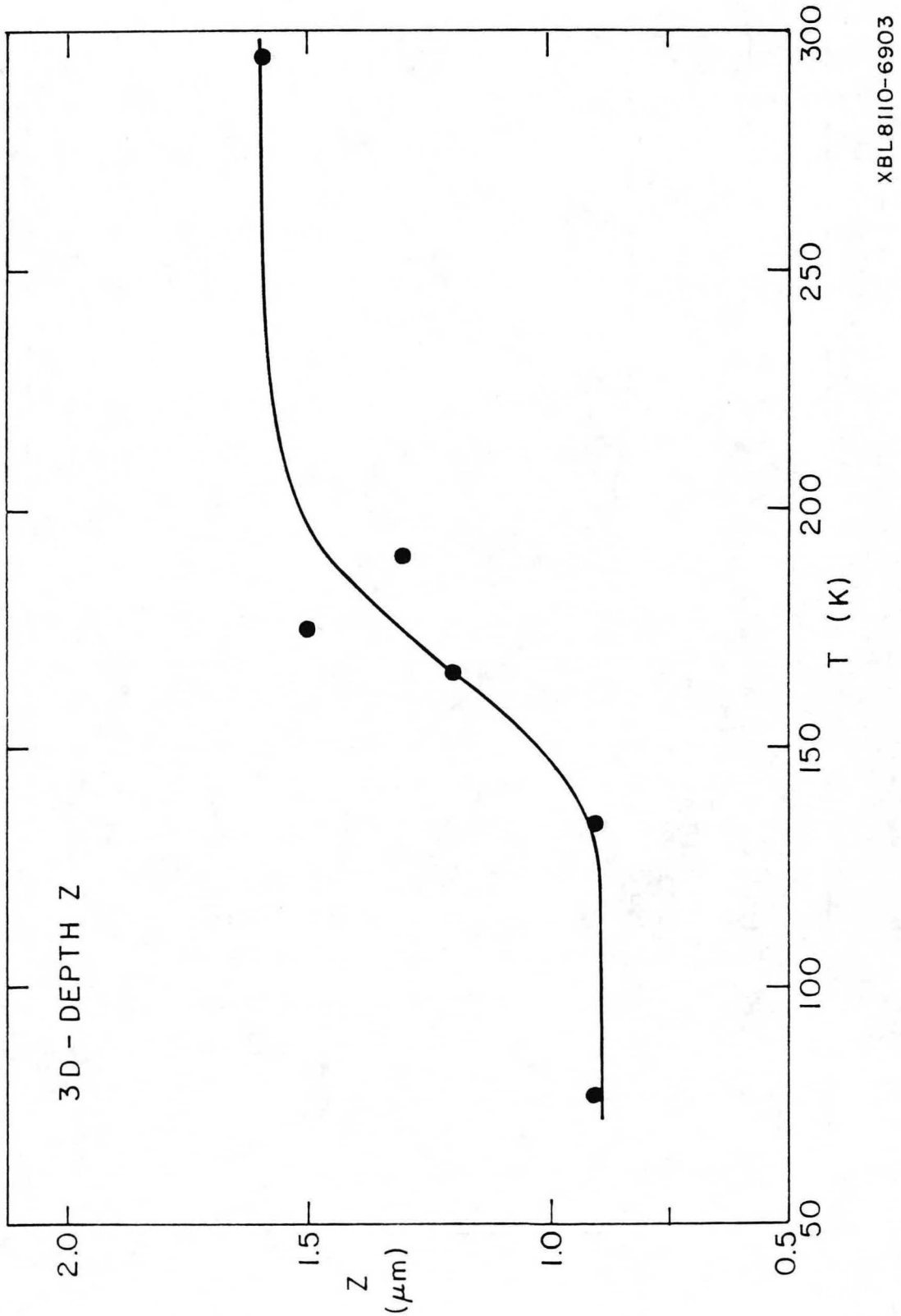

Fig. 7.

Average of maximum depth *vs.* temperature.

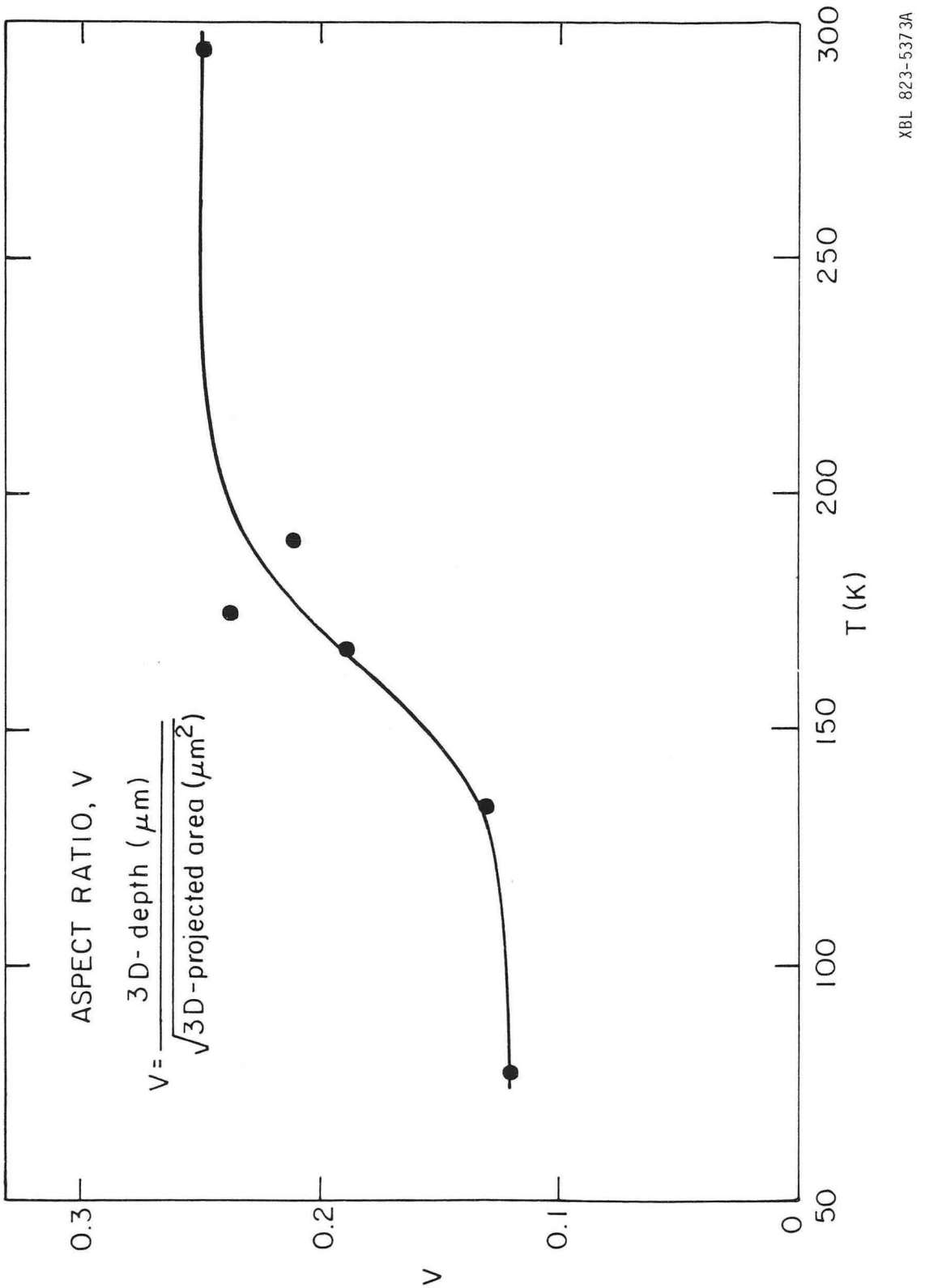

Fig. 8.

Average aspect ratio *vs.* temperature.

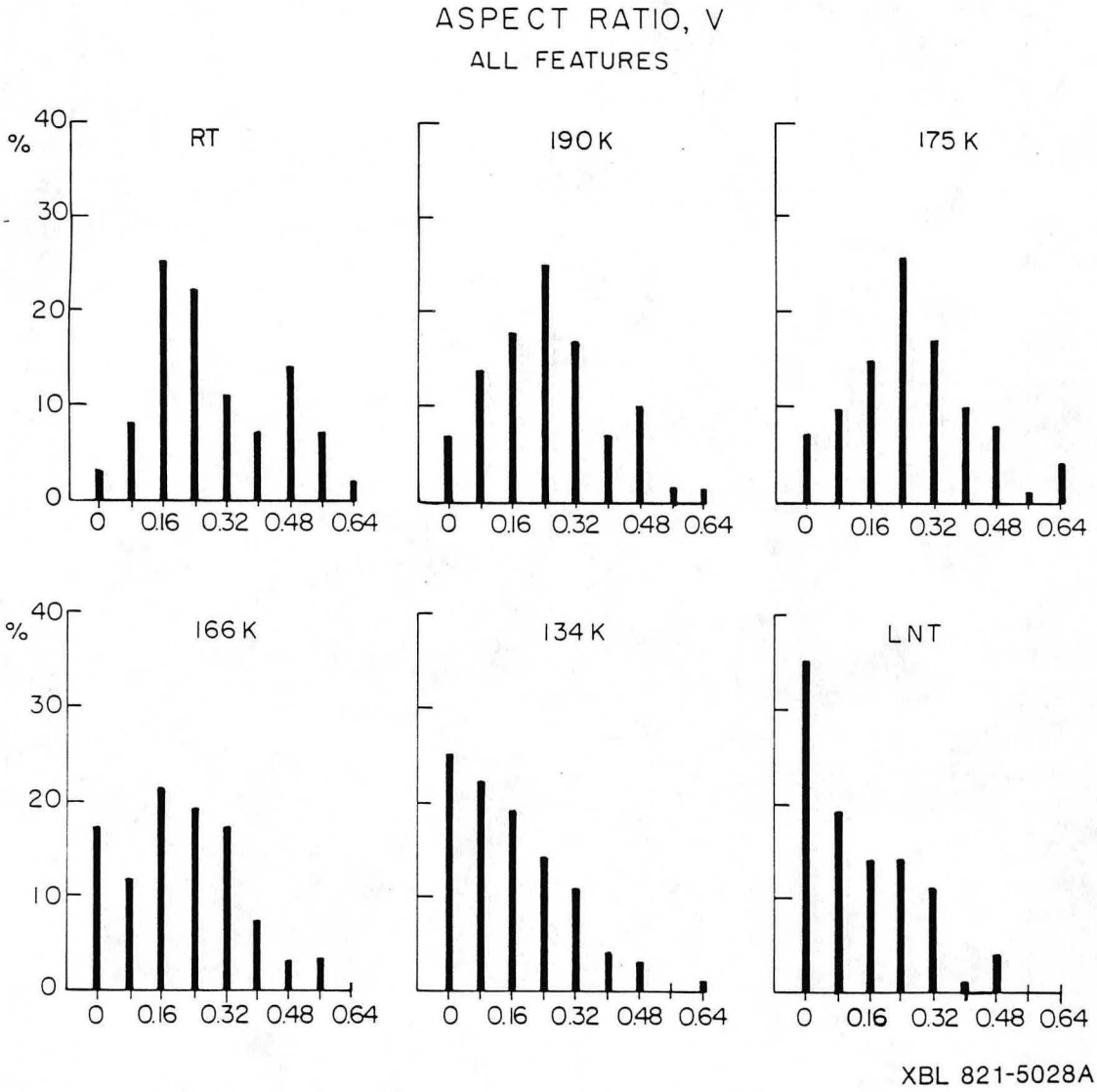

Fig. 9.

Histograms of the aspect ratio for all features.

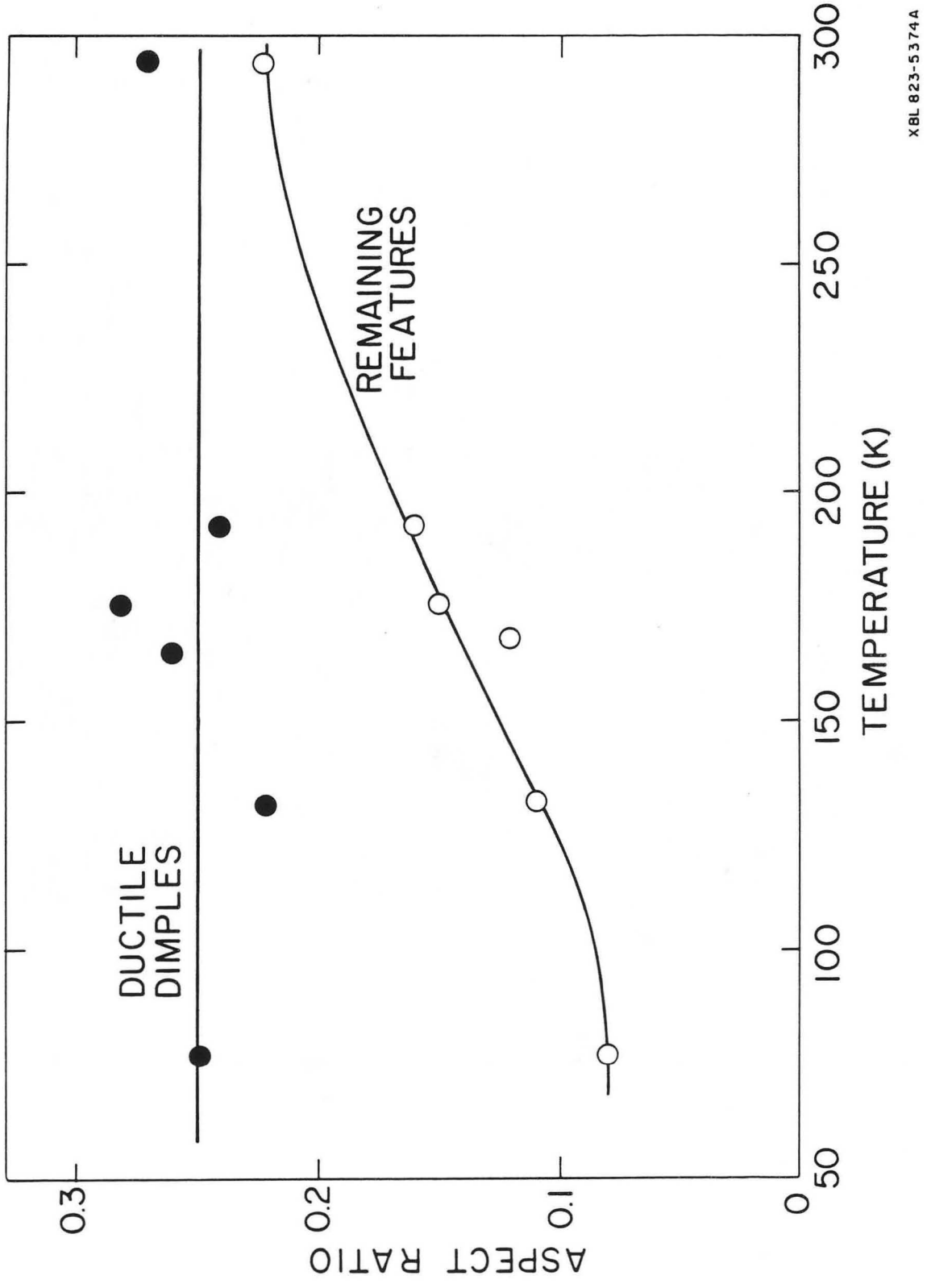

Fig. 10.

Average aspect ratio for *DD* and *RF vs.* temperature.

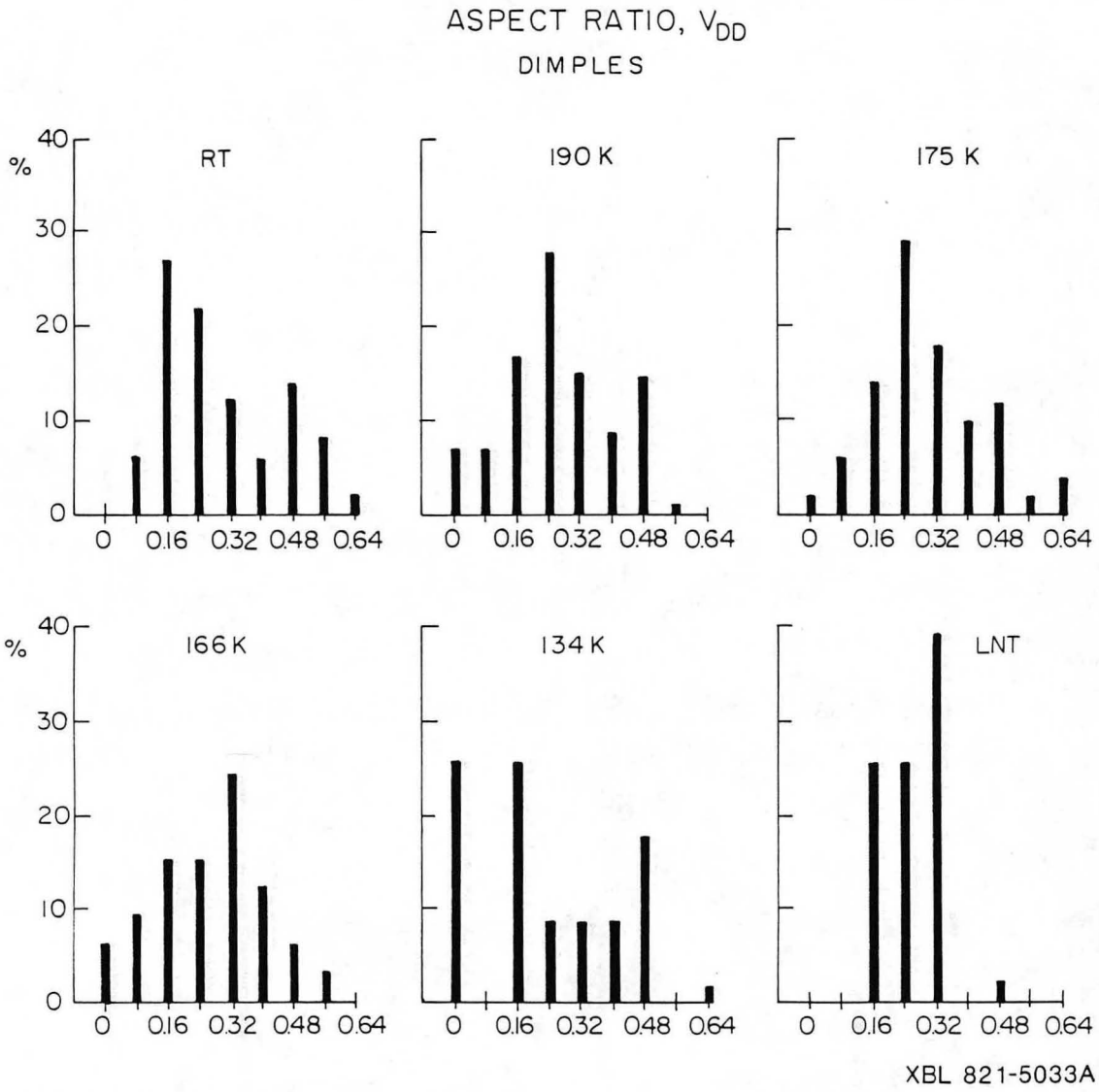

Fig. 11.

Histograms of the aspect ratio for *DD*.

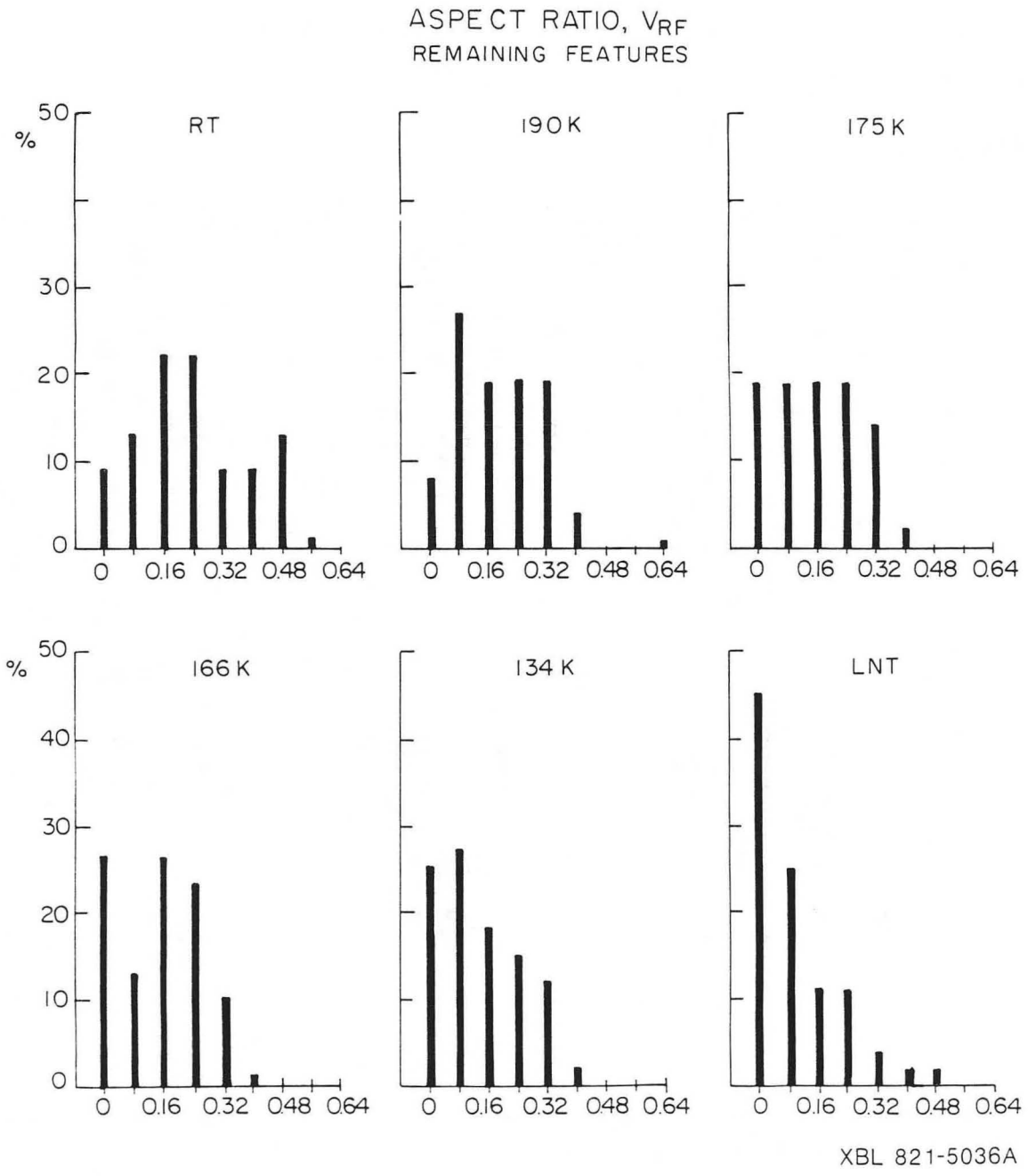

Fig. 12.

Histograms of the aspect ratio for *RF*.

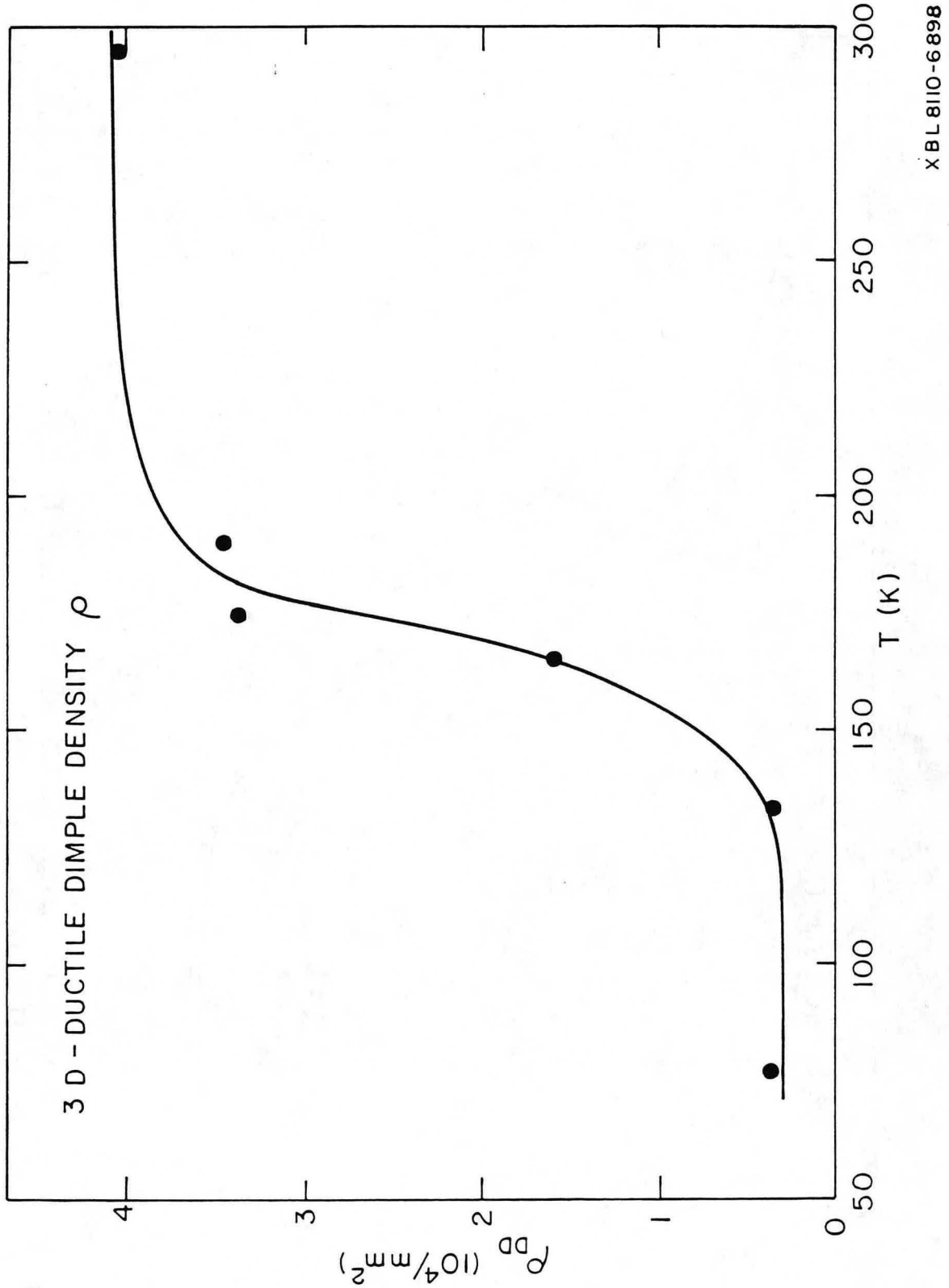

Fig. 13.

Ductile dimple density *vs.* temperature.

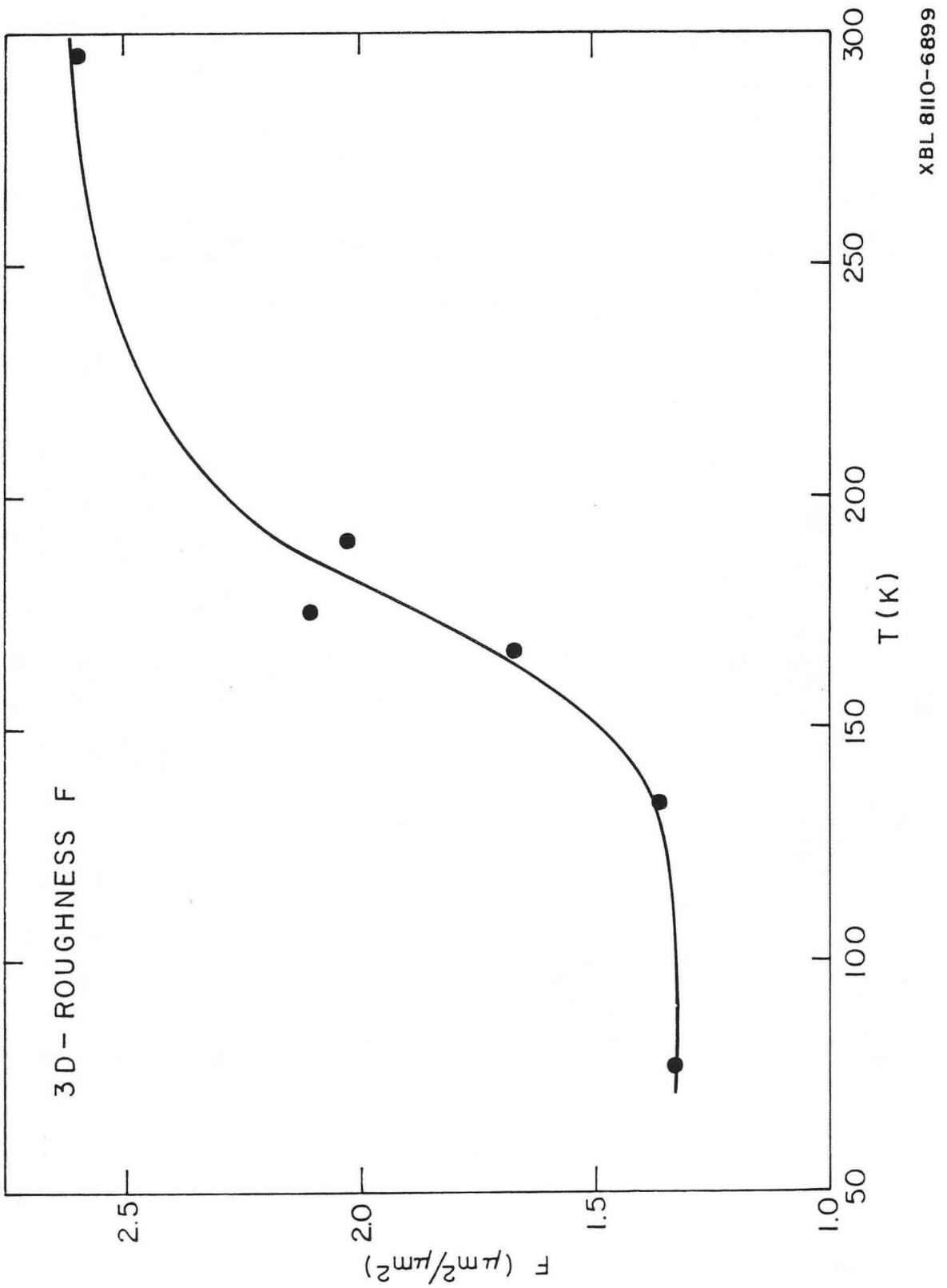

Fig. 14.

Roughness factor *vs.* temperature.

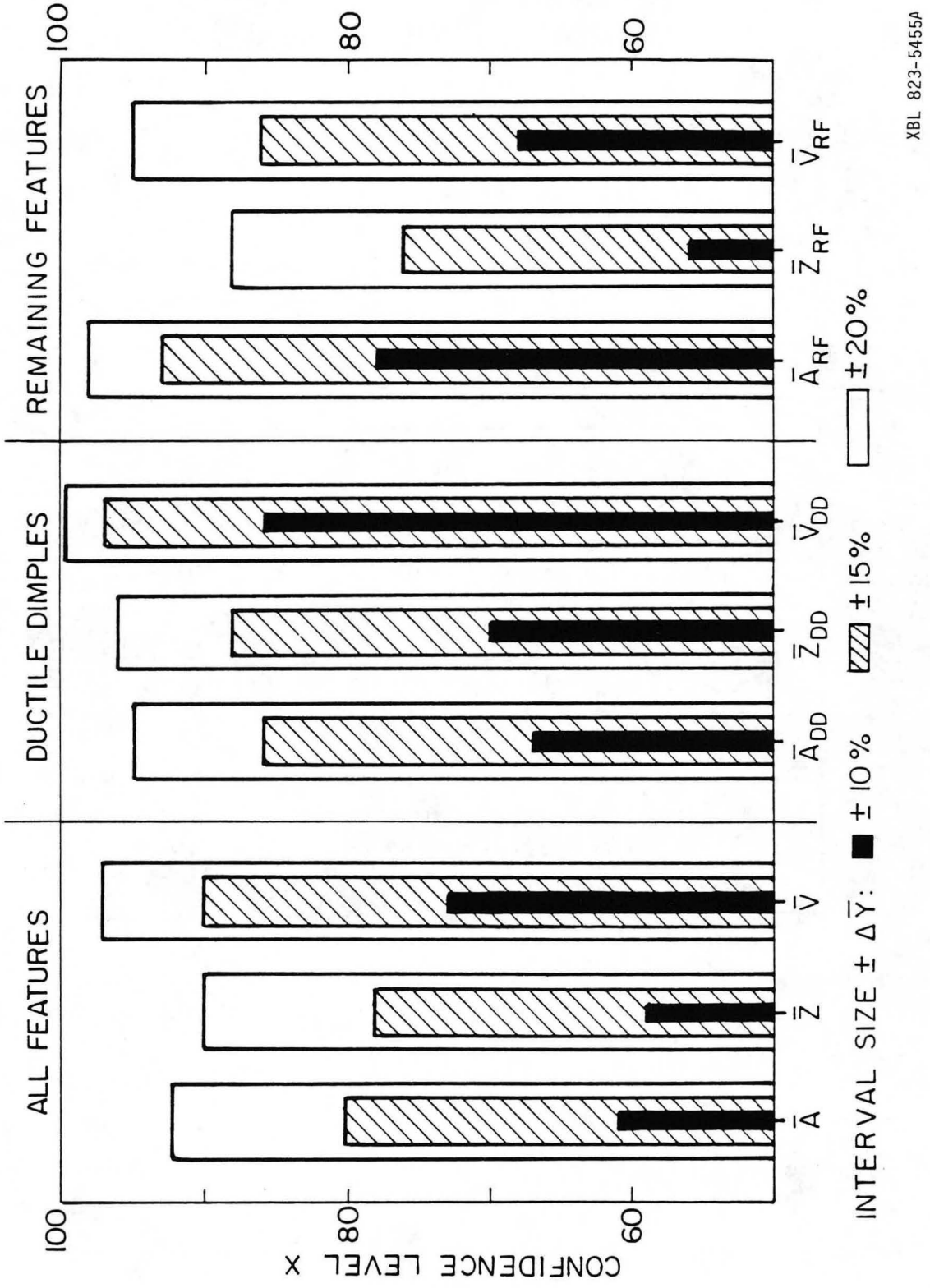

Fig. 15.

Confidence levels for mean values of A,Z and V.

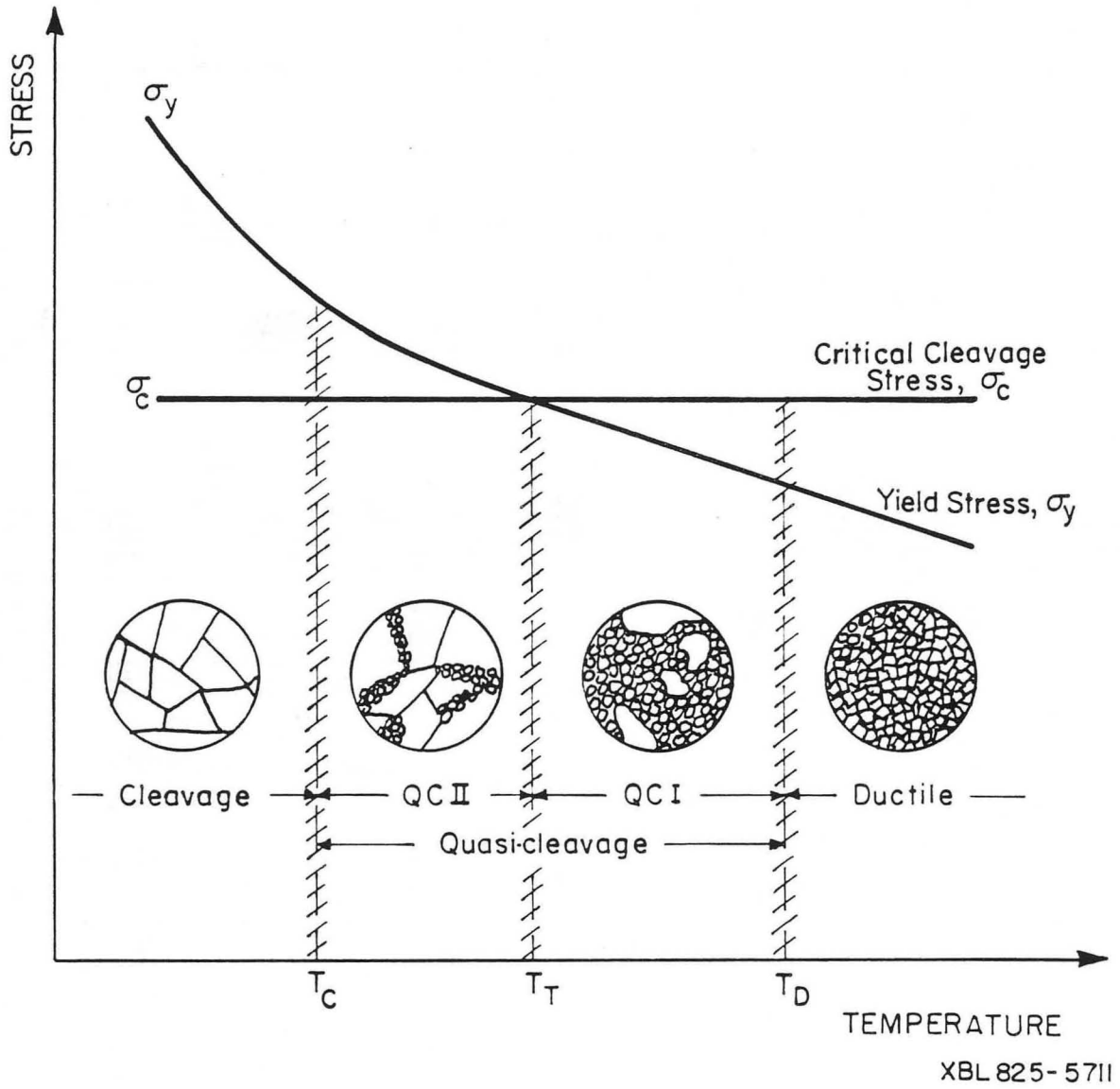

Fig. 16.

Qualitative stress-temperature dependence and fracture modes predominance.

TECHNICAL INFORMATION DEPARTMENT
LAWRENCE BERKELEY LABORATORY
UNIVERSITY OF CALIFORNIA
BERKELEY, CALIFORNIA 94720